2025 9th International Symposium on Instrumentation Systems, Circuits and Transducers (INSCIT) | 979-8-3315-9703-0/25/$31.00 ©2025 IEEE | DOI: 10.1109/INSCIT66472.2025.11181023

Silicon Sensor Characterization Testbench using the Transient Current Technique

Vinícius Fuchshuber dos Santos
Braz. Cent. Res. Phys. (CBPF) &
Mil. Inst. Eng. (IME)
Rio de Janeiro, Brazil
vinifux@gmail.com

Antonio Vilela Pereira
HEP Coord.
Braz. Cent. Res. Phys. (CBPF)
Rio de Janeiro, Brazil
antonio.vilela.pereira@cern.ch

Jorge Amaral
Dept. Elect. and Telecomm. Eng.
Rio de Janeiro State Univ. (UERJ)
Rio de Janeiro, Brazil
jamaral@eng.uerj.br

Tiago Quirino
Dept. Elect. Eng.
Rio de Janeiro State Univ. (UERJ)
Rio de Janeiro, Brazil
tiago.quirino@cern.ch

Isabella Florêncio
Elect. Eng. Grad. Prog.
Rio de Janeiro State Univ. (UERJ)
Rio de Janeiro, Brazil
isabella.fcs@gmail.com

Gabriel Bastos
Braz. Cent. Res. Phys. (CBPF) &
Fed. Cent. Tech. Educ. (CEFET-RJ)
Rio de Janeiro, Brazil
gdasbastos@gmail.com

Clemencia Mora
HEP Coord.
Braz. Cent. Res. Phys. (CBPF)
Rio de Janeiro, Brazil
clemencia.mora.herrera@cern.ch

André Massafferri
HEP Coord.
Braz. Cent. Res. Phys. (CBPF)
Rio de Janeiro, Brazil
massafferri@cbpf.br

***Abstract*—The realization of a testbench for the characterization of silicon sensors using the Transient Current Technique (TCT) is presented. The experimental setup relies on near infrared (IR) pulsed laser light with very short pulses and a localized beam spot which mirror the passage of a minimum ionizing particle (MIP) through the sensor. The setup is able to characterize sensors used in radiation detection with high spatial precision of the order of few μm along with high resolution in the time domain. The testbench is especially aimed at the characterization of silicon sensors peforming simultaneous spatial and time reconstruction for experiments running in the future upgrade of the Large Hadron Collider (LHC) particle accelerator at the European Organization for Nuclear Research (CERN).**

***Index Terms*—Silicon sensors, Radiation detection, Transient Current Technique, Low Gain Avalanche Diode, Fast timing, HL-LHC**

I. Introduction

The transient current technique (TCT) (see Refs. [1]–[3] for an overview of the technique) is widely used in the characterization of silicon radiation sensors. The analysis of the induced current pulse from the drift of non-equilibrium charge carriers allows the measurement of the drift velocity and electric field as well as the determination of the full depletion voltage, the charge collection efficiency and the effective trapping time.

TCT measurements are performed using a pulsed laser source which generates charge carriers in the silicon device. While light in the red wavelength range has short penetration length (few μm) and may be used for the study of single carrier type properties, near infrared (IR) light ($\lambda \lessapprox 1100\,\text{nm}$) mimics the charge generation profile of minimum ionizing particles (MIP) with ionization along the direction of the beam with penetration from tens to hundreds of μm.

The technique is suited for the characterization of sensors designed for high-precision time measurements, such as those used in particle physics experiments (e.g. Ref. [4]) and in X-ray detection from synchrotron light sources (see Ref. [5] for a recent application). Sensors that feature high resolution both spatially and in time, and hence allow reconstruction of trajectories in *4 dimensions*, are particularly important in experiments that will run in the future upgrade of the Large Hadron Collider (LHC)—the High-Luminosity LHC (HL-LHC)—and other future particle physics accelerators (see Refs. [6], [7] for reviews of two such technologies).

This paper describes the testbench assembled for TCT measurements at the Brazilian Center for Research in Physics (CBPF), with representative results from its operation and time resolution measurements for fast silicon sensors. This is the first testbench in Brazil aimed at the characterization of fast silicon sensors for particle physics and related applications using TCT measurements.

II. Experimental setup

A. Laser system

The optical testbench is shown in Fig. 1. The laser generates pulses with width $< 100\,\text{ps}$ and jitter $\lessapprox 3\,\text{ps}$. The laser controller outputs a reference signal that can be used as trigger for the data acquisition. The laser is fiber-coupled with minimal attenuation and reflection. The laser output is sent

through an adjustable attenuator and a fiber splitter/coupler. Two fiber couplers may be used: 1) with a fraction of the light output directed to a photodiode for the monitoring of the pulse height and 2) in a loopback configuration such that the pulse repetition is used as reference for the time measurement, eliminating the jitter from the source. The light output is collimated. The focusing system uses a Galilean beam expander and a focusing lens. The picosecond laser pulses reach the device under test (DUT) with a beam spot size $\lessapprox 10\,\mu$m.

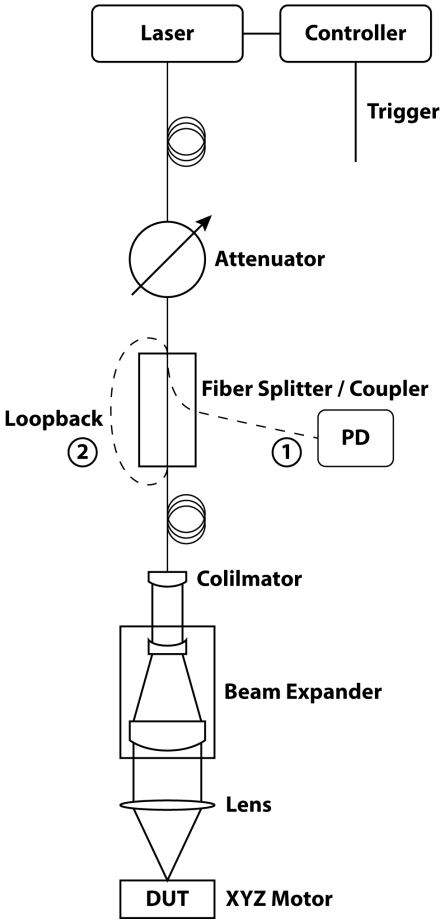

Fig. 1. Schematic diagram of the optical testbench. The two labeled alternative paths (1 & 2) correspond to the monitoring with a photodiode (PD) and the loopback into the fiber coupler. The laser beam is focused in the device under test (DUT) attached to an XYZ motorized translation stage.

The DUT is attached to an XYZ motorized translation stage with resolution of $\mathcal{O}(1\,\mu\text{m})$. The DUT is moved with high precision in the plane perpendicular to the beam, taken as the XY plane, for one- or two-dimensional position scans of the beam on the device's surface, and in the direction of the beam (the Z direction) for focusing.

The position and focusing scans are automated by a remote application, allowing for an efficient operation and data taking. The application's Graphical User Interface (GUI) is shown in Fig. 2.

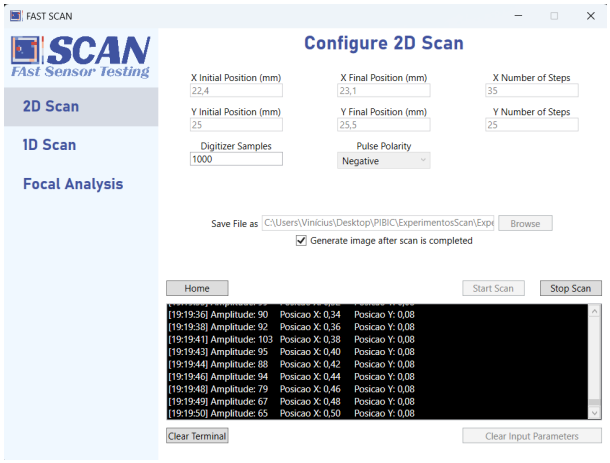

Fig. 2. Graphical User Interface (GUI) view for automatic measurements including position scans in one and two coordinates.

B. Low Gain Avalanche Diode sensors and readout

The laser setup allows a precise characterization of the sensor device response as a function of the position of the incoming excitation. Moreover, by using pulses of short duration, the setup is particularly suited for measuring the sensor characteristics in the time domain.

The IR laser pulse of short duration and focused in a small beam spot mimics the passage of particles/radiation through the sensor which generate electron-hole pairs in their path.

Low Gain Avalanche Diode (LGAD) sensors are especially suited for particle and radiation detection in time-sensitive applications (see Refs. [8]–[11] for a review of LGAD sensors and their performance). The LGAD doping profile is depicted in Fig. 3. In addition to a p-i-n structure on a high-resistivity bulk, a p+ layer is implanted below the n++ electrode. When reversely biasing the sensor, a high electric field—with respect to that in the remaining active volume—is produced across the p+ implant, enabling charge multiplication and a gain of up to $\mathcal{O}(100)$. The LGAD sensor is designed for linear response, with an electrical signal proportional to the energy deposited by the incoming radiation. LGAD sensors are typically thin, with an active depth of $\sim 50\,\mu$m whereas traditional silicon sensors feature depths of hundreds of μm. The smaller thickness gives rise to a short drift time ($\lessapprox 1\,$ns) for an improved timing performance. The sensor gain balances the smaller number of electron-hole pairs generated in a thin sensor by the impinging radiation, giving the sensor high energy resolution. A reverse bias at high voltage improves the sensor response and time resolution.

For the results shown in this paper, LGAD sensors fabbricated by Hamamatsu Photonics (HPK) were used. The 2x2 multi-pad sensors feature pad sizes of $1.3 \times 1.3\,\text{mm}^2$. The metalized back of the sensor corresponging to the p++ anode electrode is attached to a PCB using a high-conductivity epoxy. A negative high-voltage bias is applied to the sensor anode. One channel is read-out via the cathode into an on-board transimpedance amplifier stage with large analog bandwidth

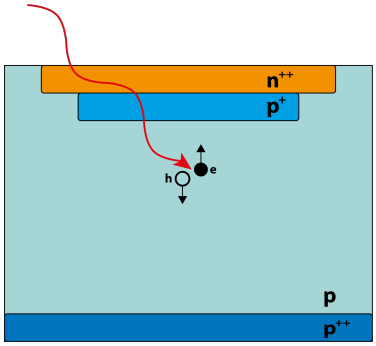

Fig. 3. Sketch of the cross-sectional view of a Low Gain Avalanche Diode (LGAD). When depleted, the moderately doped p+ implant below the n++ electrode produces a high electric field capable of inducing charge multiplication.

and low noise. The electrical signal from the sensor board is fed to a large bandwidth, low noise RF amplifier with a frequency-dependent gain in the vicinity of 20 dB.

The sensors are fabbricated with a top metal and SiO_2 passivation layers that block the laser beam into the silicon substrate. Small openings in the metal and passivation layers are however included which allow the stimulation of the sensor active area by the laser. An HPK 2x2 LGAD sensor, attached to a PCB, is shown in Fig 4, where the signal pads and laser openings are visible.

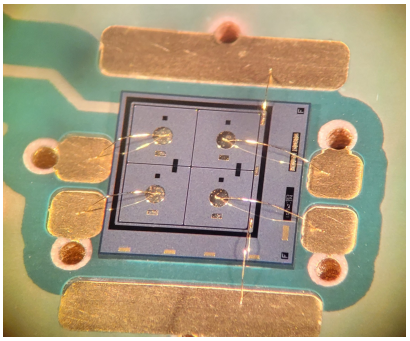

Fig. 4. LGAD sensor attached to a PCB with signal pads wire-bonded for readout.

The Data Acquisition (DAQ) consists of a large analog bandwidth, high sampling rate (5 GSa/s) waveform digitizer transmitting at large data bandwidth and of an oscilloscope with very large analog bandwidth (12.5 GHz) and sampling rate (100 GSa/s). The acquisition is triggered by the reference signal from the laser controller. Fig. 5 shows a representative waveform of the digitalized signal when the LGAD sensor is stimulated by an input IR laser pulse.

C. Beam focusing

The beam focusing relies on the measurement of the beam width at the sensor device. The measurement of the beam width is best performed using a metal-silicon sharp edge, as in the openings in the metalization and passivation layers of the sensor.

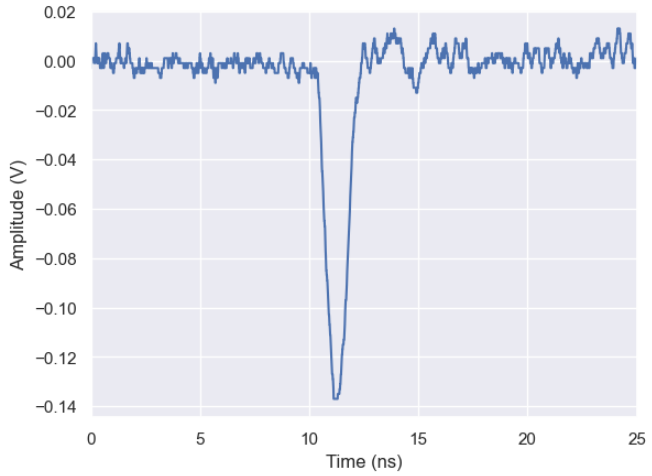

Fig. 5. Recorded waveform of the LGAD sensor corresponding to one pulse of the IR laser beam.

Fig. 6 illustrates the method. As the device is moved in one direction such that the beam spot is brought within the opening, the average charge induced in the sensor increases in proportion to the beam intensity to which the sensor is exposed.

The average peak amplitude is calculated for a large number of measurements, versus the beam position with respect to the sensor. The beam width is measured from a fit to an *S-curve*, assuming a Gaussian beam profile.

The beam width is measured while moving the device in incremental steps in the beam direction in order to reach the optimal beam spot size.

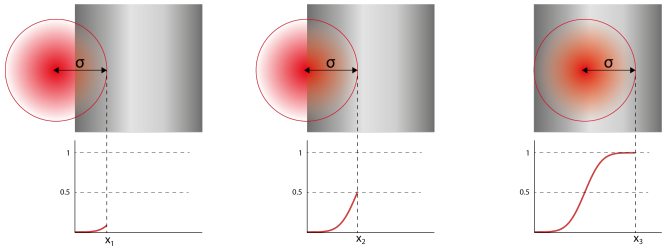

Fig. 6. Sketch of the beam width measuring method. The opening in the passivation and metalization layers of the sensor is represented by the gray square. The sensor is moved such that in each step a larger fraction of the beam intensity enters the silicon substrate across the metal-silicon edge.

III. Results

A. Two-dimensional scan

Fig. 7 shows a two-dimensional scan of the sensor device in an area of roughly $700 \times 500\,\mu$m around the laser openings. One channel of the sensor is read-out, as discussed in Sect. II-B. The two openings in one pad are clearly observed (cf. Fig. 4).

B. Beam focusing and spot size

The results of the beam focusing scan using the LGAD sensor are shown in Fig. 8. At each step along the beam

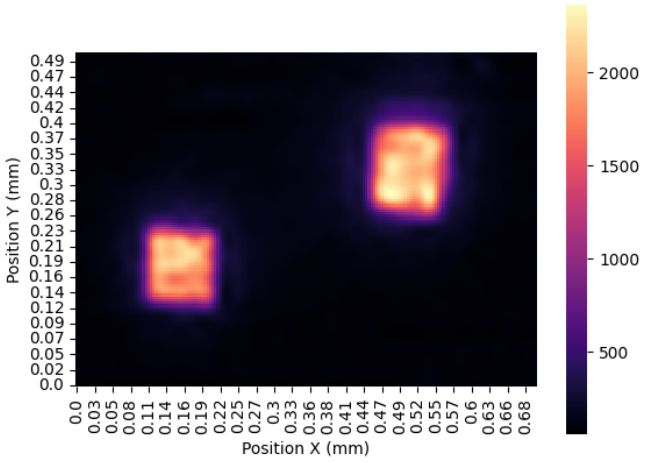

Fig. 7. Two dimensional scan showing a section of one pad of the LGAD sensor. Two openings in the passivation and metalization layers of the sensor are clearly observed; they are sensitive to the IR laser beam.

direction, an S-curve is obtained from a fit to the one-dimensional scan where the beam is brought into an opening. As the sensor is moved in the beam direction, it reaches the optimal focus, represented by an S-curve with sharper turn-on and smaller measured beam width. When the sensor is placed away from the focus position, the turn-on of the S-curve is broader, corresponding to a larger beam width.

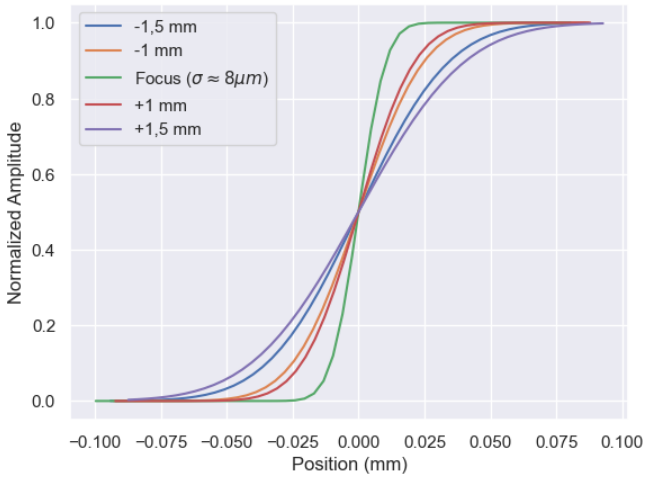

Fig. 8. Results of the focusing procedure using the LGAD sensor. As the sensor is brought closer to the optimal focus, the S-curve of the scan shows a sharper turn-on. The S-curve fit gives an estimate of the beam spot size.

C. Sensor characterization and time resolution

The sensor characteristics are obtained with the beam spot moved to the center of the laser opening, where the distance to the opening edge is several times the beam width. The laser intensity is adjusted such that the average signal amplitude correlates to that obtained by stimulating the sensor using a radiation source. The signal amplitude from the LGAD sensor is calibrated using a ^{90}Sr beta source, which produces MIPs passing through the sensor. The amplitude calibration measurement with the ^{90}Sr source is performed using the same readout chain, explained in Sect. II-B.

By measuring the time difference between the pulse rising edge time and a reference time—or between the main pulse and its attenuated copy when in the loopback configuration (see Sect. II-A)—the sensor time resolution can be measured.

Fig. 9 shows the distribution of the time difference between the LGAD pulse and the reference trigger from the laser controller, when the sensor is biased at a lower high-voltage value (120 V). The distribution shows a Gaussian shape and the time resolution is obtained by fitting the distribution, resulting in a resolution of $\sigma_{\Delta t} \approx 25$ ps. Increasing the high-voltage biasing the sensor, the time resolution is expected to improve. At 150 V, the time resolution was measured as $\sigma_{\Delta t} \approx 20$ ps.

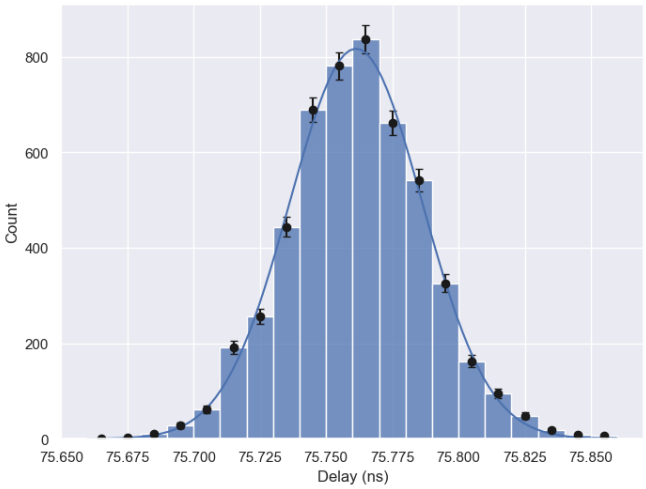

Fig. 9. Distribution of the time difference between the pulse rising edge time and the reference trigger for the LGAD sensor, with the sensor biased at one operating point.

The pulse time measurement is performed at a threshold defined as a function of the amplitude, approximately canceling the effect of time walk. The charge distribution generated in the sensor is a random process (Landau fluctuations) leading to amplitude as well as shape variations of the induced current in the electrodes. While amplitude variations that produce the time walk effect can be accounted for, the shape variations to the signal degrade the time resolution. The impact from Landau fluctuations are reduced by steep signal rise times as in LGAD sensors. The time resolution is affected by jitter due to noise. This contribution to the time resolution is inversely proportional to the slope of the signal and hence increases with the pulse rise time. It is inversely proportional to the signal-to-noise ratio. The time resolution may also be degraded by distortions to the signal shape due to a non-uniform drift velocity or weighting field.

IV. Conclusion and Outlook

The highly focused beam on the DUT, as well as high spatial and time resolution of the setup allow for a range of TCT

measurements. The laser and optical setup are interchangeable in order to use beams of different wavelengths.

By using a beam with small pulse widths and relatively large penetration length, the sensor response to the laser input is similar to that from MIPs, relevant for radiation detectors.

The fast laser pulses with low jitter, along with measurements at large sample rate, make the testbench suited for the characterization of the sensor signal output in the time domain. The sensor induced current and the pulse time resolution—essential for time-sensitive applications—can be measured with high precision.

The automation of the focusing, spatial and time measurements enables a short turnaround and reproducibility of the characterization results.

Silicon sensors are required to operate a low temperatures, especially when exposed to large radiation doses. While the testbench currently operates at room temperature, cooling of the sensor to typical sub-zero operating temperatures is foreseen.

ACKNOWLEDGMENTS

The authors extend their gratitude to Roberta Arcidiacono and Nicolò Cartiglia for their invaluable assistance.

The authors are thankful to the Industrial Networks and Automation Systems Laboratory (LARISA) and the Nanofabrication Laboratory (NANOFAB) at Rio de Janeiro State University (UERJ), the HEP Laboratory and the Laboratory of Instrumentation and Mechanical Technology (LITMec) at Brazilian Center for Research in Physics (CBPF), and the Eldorado Research Institute.

This work has been supported by the Carlos Chagas Filho Research Support Foundation (FAPERJ) and the Brazilian National Council for Scientific and Technological Development (CNPq).

REFERENCES

[1] V. Eremin, N. Strokan, E. Verbitskaya and Z. Li, "Development of transient current and charge techniques for the measurement of effective net concentration of ionized charges (N_{eff}) in the space charge region of p-n junction detectors," Nucl. Instrum. Meth. A **372**, 388-398 (1996) doi:10.1016/0168-9002(95)01295-8

[2] V. Eremin, Z. Li and I. Ilyashenko, "Trapping induced N_{eff} and electrical field transformation at different temperatures in neutron irradiated high resistivity silicon detectors," Nucl. Instrum. Meth. A **360**, 458-462 (1995) doi:10.1016/0168-9002(95)00112-3

[3] G. Kramberger, V. Cindro, I. Mandic, M. Mikuz and M. Zavrtanik, "Determination of effective trapping times for electrons and holes in irradiated silicon," Nucl. Instrum. Meth. A **476**, 645-651 (2002) doi:10.1016/S0168-9002(01)01653-9

[4] H. F. W. Sadrozinski, S. Ely, V. Fadeyev, Z. Galloway, J. Ngo, C. Parker, B. Petersen, A. Seiden, A. Zatserklyaniy and N. Cartiglia, *et al.* "Ultra-fast silicon detectors," Nucl. Instrum. Meth. A **730**, 226-231 (2013) doi:10.1016/j.nima.2013.06.033

[5] S. M. Mazza, G. Saito, Y. Zhao, T. Kirkes, N. Yoho, D. Yerdea, N. Nagel, J. Ott, M. Nizam and M. Leite, *et al.* "Synchrotron light source X-ray detection with Low-Gain Avalanche Diodes," JINST **18**, no.10, P10006 (2023) doi:10.1088/1748-0221/18/10/P10006 [arXiv:2306.15798 [physics.ins-det]].

[6] V. Sola, R. Arcidiacono, A. Bellora, N. Cartiglia, F. Cenna, R. Cirio, S. Durando, M. Ferrero, Z. Galloway and B. Gruey, *et al.* "Ultra-Fast Silicon Detectors for 4D tracking," JINST **12**, no.02, C02072 (2017) doi:10.1088/1748-0221/12/02/C02072

[7] A. Lai, L. Anderlini, M. Aresti, A. Bizzeti, A. Cardini, G. F. Dalla Betta, G. T. Forcolin, M. Garau, A. Lampis and A. Loi, *et al.* "First results of the TIMESPOT project on developments on fast sensors for future vertex detectors," Nucl. Instrum. Meth. A **981**, 164491 (2020) doi:10.1016/j.nima.2020.164491

[8] G. Pellegrini, P. Fernández-Martínez, M. Baselga, C. Fleta, D. Flores, V. Greco, S. Hidalgo, I. Mandić, G. Kramberger and D. Quirion, *et al.* "Technology developments and first measurements of Low Gain Avalanche Detectors (LGAD) for high energy physics applications," Nucl. Instrum. Meth. A **765**, 12-16 (2014) doi:10.1016/j.nima.2014.06.008

[9] N. Cartiglia, R. Arcidiacono, M. Baselga, R. Bellan, M. Boscardin, F. Cenna, G. F. Dalla Betta, P. Fernndez-Martnez, M. Ferrero and D. Flores, *et al.* "Design optimization of ultra-fast silicon detectors," Nucl. Instrum. Meth. A **796**, 141-148 (2015) doi:10.1016/j.nima.2015.04.025

[10] V. Sola, R. Arcidiacono, M. Boscardin, N. Cartiglia, G. F. Dalla Betta, F. Ficorella, M. Ferrero, M. Mandurrino, L. Pancheri and G. Paternoster, *et al.* "First FBK production of 50 μm ultra-fast silicon detectors," Nucl. Instrum. Meth. A **924**, 360-368 (2019) doi:10.1016/j.nima.2018.07.060 [arXiv:1802.03988 [physics.ins-det]].

[11] R. Heller, A. Abreu, A. Apresyan, R. Arcidiacono, N. Cartiglia, K. DiPetrillo, M. Ferrero, M. Hussain, M. Lazarovitz and H. Lee, *et al.* "Combined analysis of HPK 3.1 LGADs using a proton beam, beta source, and probe station towards establishing high volume quality control," Nucl. Instrum. Meth. A **1018**, 165828 (2021) doi:10.1016/j.nima.2021.165828 [arXiv:2104.08369 [physics.ins-det]].